scientific reports

Check for updates

OPEN

Synthesis and application of diazenyl sulfonamide-based schiff bases as potential BRCA2 active inhibitors against MCF-7 breast cancer cell line

Olia Rezaeianzadeh[1], Sakineh Asghari[1]✉, Mahmood Tajbakhsh[1], Asieh Khalilpour[2] & Sergey Shityakov[3]

In this study, a library of novel sulfonamide-based Schiff bases 3a-j was synthesized in high yield (75 to 89%). The FTIR, ^{1}H NMR, and ^{13}C NMR spectroscopic techniques and mass analysis were used to characterize the synthesized compounds. Their anticancer activity was assessed in vitro on the breast cancer (MCF-7) and healthy human breast epithelial (MCF-10 A) cell lines over 48 and 72 h using the MTT assay. Most of the synthesized compounds demonstrated promising activity, with compound 3i showing particularly high efficacy at 48 and 72 h (IC_{50} = 4.85 ± 0.006 and 4.25 ± 0.009 µM) against the MCF-7 breast cancer cell line. Furthermore, molecular docking studies were performed for compounds 3a-j with the PDB: (3UV7) protein of the breast cancer susceptibility gene 2 (BRCA2). The obtained results revealed that compound 3i has the strongest binding affinity energy (-7.99 kcal/mol), consistent with the obtained experimental data. Additionally, molecular dynamics (MD) simulation assays confirm the formation of a stable 3i-BRCA2 complex with strong binding affinity through the formation of hydrogen bonds. Antioxidant activities were determined by in vitro assay DPPH cation radical activity method. Interestingly, the compound 3j (IC_{50} = 12.36 ± 0.55 µM) had comparable activity with ascorbic acid (IC_{50} = 13.58 ± 0.38 µM) in the antioxidant assay. The results of this research could potentially contribute to the development of new therapeutic agents useful in fighting caused by breast cancer.

Keywords Sulfonamides, Sulfonamide-based schiff base, MCF-7 breast cancer cell line, BRCA2, Cytotoxicity

Breast cancer is a complex disease that includes various tumor subtypes with unique histological features and diverse clinical manifestations[1]. About 2.3 million patients are diagnosed with breast cancer annually, leading to over 670,000 deaths. In the United States, an anticipated 287,850 new instances of female breast cancer were recorded in 2022, with 43,250 reported deaths[2,3]. Approximately 30–40% of breast cancer patients develop metastases to numerous vital organs, such as the lungs, brain, liver, and bone, which can ultimately result in death despite standard treatment[4]. Although significant progress has been made in cancer chemotherapy, the current drugs used in treatment still show limited therapeutic efficacy[5]. Resistance in various cancer types has led to palliative responses, rather than curative outcomes[6]. The impact of cancer therapies on mortality rates has not met expectations[7]. Targeted therapy focusing on cancer-specific molecules and signaling pathways has shown reduced toxic effects compared to chemotherapy[8]. Even though advancements in treatment and early detection have improved survival rates, the quality of life for patients is often compromised by cancer and its treatments[9].

Presently, approximately 5–10% of breast cancer cases are directly associated with inherited conditions caused by mutations in specific susceptibility genes[10]. The breast cancer susceptibility gene 2 (BRCA2) is notably identified as the primary high-risk factor for breast cancer[11].

The primary sulfonamide molecule is a crucial structure found in many important bioactive and medicinal compounds with various pharmacological medicine functions such as antibacterial[12], antiviral[13], hypoglycemic[14],

[1]Department of Organic Chemistry, Faculty of Chemistry, University of Mazandaran, Babolsar 47416- 95447, Iran. [2]Department of Environmental Health Engineering, Babol University of Medicinal Sciences, Babol, Iran. [3]Infochemistry Scientific Center, ITMO University, Lomonosova str. 9, 191002 Saint Petersburg, Russia. ✉email: s.asghari@umz.ac.ir

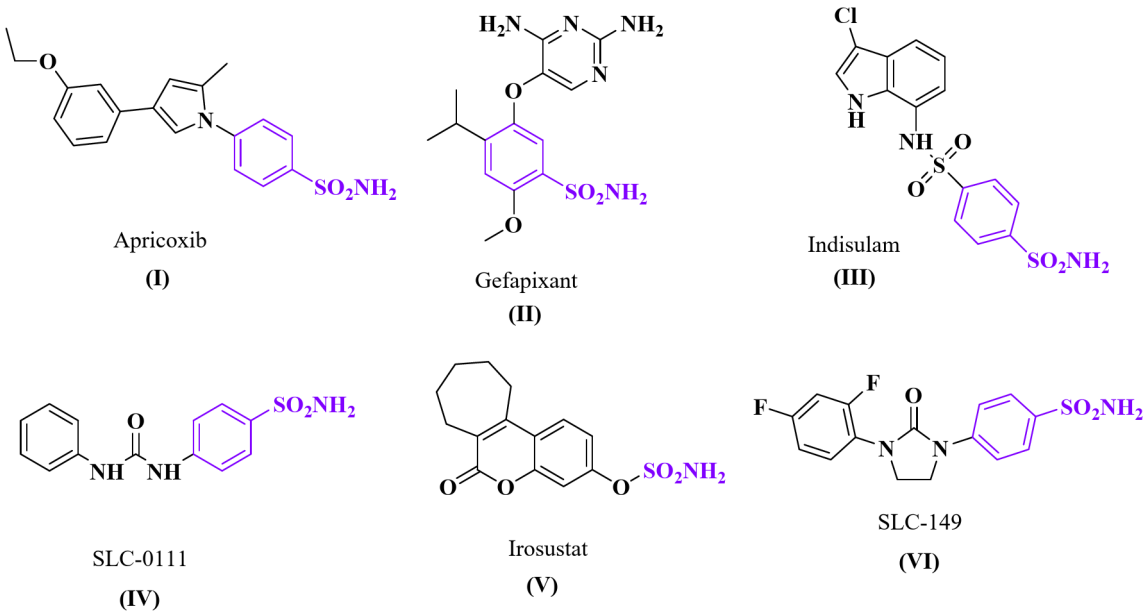

Fig. 1. Some anticancer drugs based on primary sulfonamide.

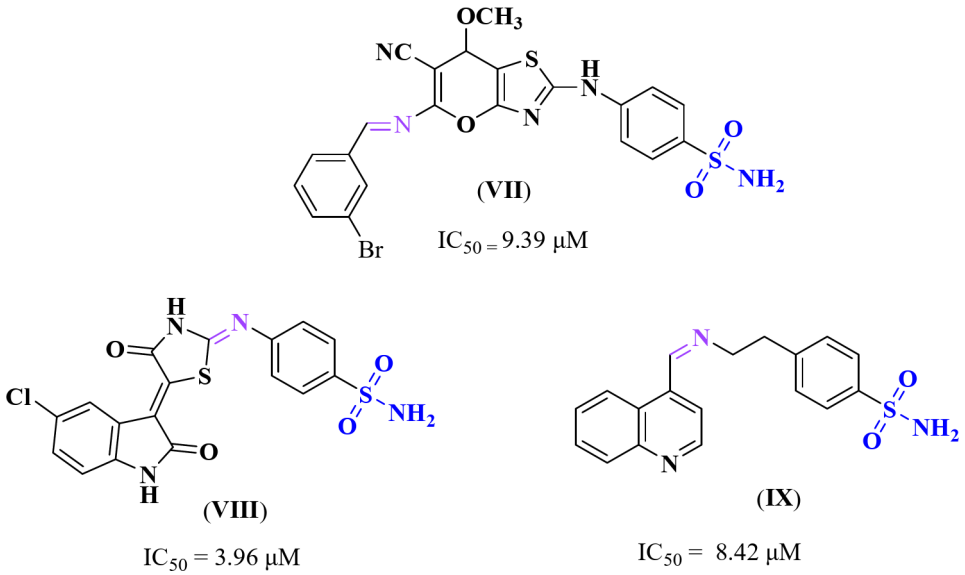

Fig. 2. Reported sulfonamide-based Schiff bases with potent MCF-7 activity.

antithyroid[15], anti-inflammatory[16], and diuretic effects[17]. Additionally, sulfonamides have shown promising anticancer activity in vitro and in vivo[18]. Several marketed pharmacological medicines are available having primary sulfonamide as a core active moiety like Apricoxib (**I**)[19], Gefapixant (**II**)[20], Indisulam (**III**)[21], SLC-0111 (**IV**)[22], Irosustat (**V**)[23], and SLC-149 (**VI**)[24], which have shown anticancer properties (Fig. 1). On the other hand, primary sulfonamides without any substituents are subjected to chemical changes in the sulfonamide group, which can affect their effectiveness, absorption, and metabolism[25,26].

Furthermore, Schiff bases have demonstrated a wide range of pharmacological activities, including antimalarial[27], antiproliferative[28], analgesic[29], anti-COVID-19[30], antifungal[31], antibacterial[32], and cytotoxic effects[33]. Several sulfonamide-based Schiff base derivatives have been synthesized and evaluated for their effectiveness against different types of cancers, notably breast cancer (Fig. 2).

Ghorab et al. prepared some sulfonamide-based Schiff bases, which demonstrated anticancer activities against the MCF-7 breast cancer cell line, using the MTT assay. Among the tested samples, compound **VII** exhibited the highest anticancer activity against the MCF-7 cell line (IC_{50} = 9.27 µM)[34]. In another study, Eldehna et al. introduced a new series of oxindole derivatives of sulfonamide-based Schiff base, and their anticancer activity was evaluated against the MCF-7 breast cancer cell line. Their results exhibited that compound **VIII**

had the most cytotoxicity against MCF-7 (IC_{50} = 3.96 ± 0.21 µM) compared to the other derivatives[35]. Likewise, El-Malah et al. synthesized a new series of Schiff bases featuring a quinoline structure as the central scaffold that connected to benzenesulfonamide moiety. The anti-proliferative activity of compounds was tested against MCF-7 and MDA-MB-231 breast cancer cell lines. Among the quinoline benzenesulfonamide Schiff bases, compound I**X** demonstrated high anticancer activity against the MCF-7 cell line, with an IC_{50} of 8.42 µM[36].

In this context, we aimed to synthesize new sulfonamide-based Schiff bases (**3a-j**) by reacting an azo-based sulfonamide aldehyde (**1**) with various primary amines (**2a-j**) (Fig. 3), and evaluate their potential against breast cancer (MCF-7) and healthy human breast epithelial (MCF-10 A) cell lines. Molecular docking and molecular dynamic (MD) studies were also performed to analyze the interactions of compounds **3a-j** with the BRCA2 protein (PDB ID: 3UV7).

Experimental

Materials and instruments

The chemicals used in this study were obtained from Sigma, Aldrich, and Fluka Companies. Intermediate **1** was prepared following the procedure described previously[18]. The headway of the reactions was observed through thin-layer chromatography (TLC) utilizing silica gel plates.

A variety of methods, such as melting points, infrared (IR) spectroscopy, ^{1}H nuclear magnetic resonance (NMR) spectroscopy, ^{13}C NMR spectroscopy, and mass spectrometry, were utilized to confirm the structures of the synthesized compounds. The determination of melting points was carried out using the Electrothermal 9100 device (Keison Products, Essex, UK) in open capillary tubes. To conduct infrared spectral studies, a Bruker FT-IR (Bruker, Karlsruhe, Germany) spectrophotometer instrument was utilized with the KBr disc method, and the spectra were obtained within the range of 500–4000 cm^{-1}. The ^{1}H NMR and ^{13}C NMR spectra were

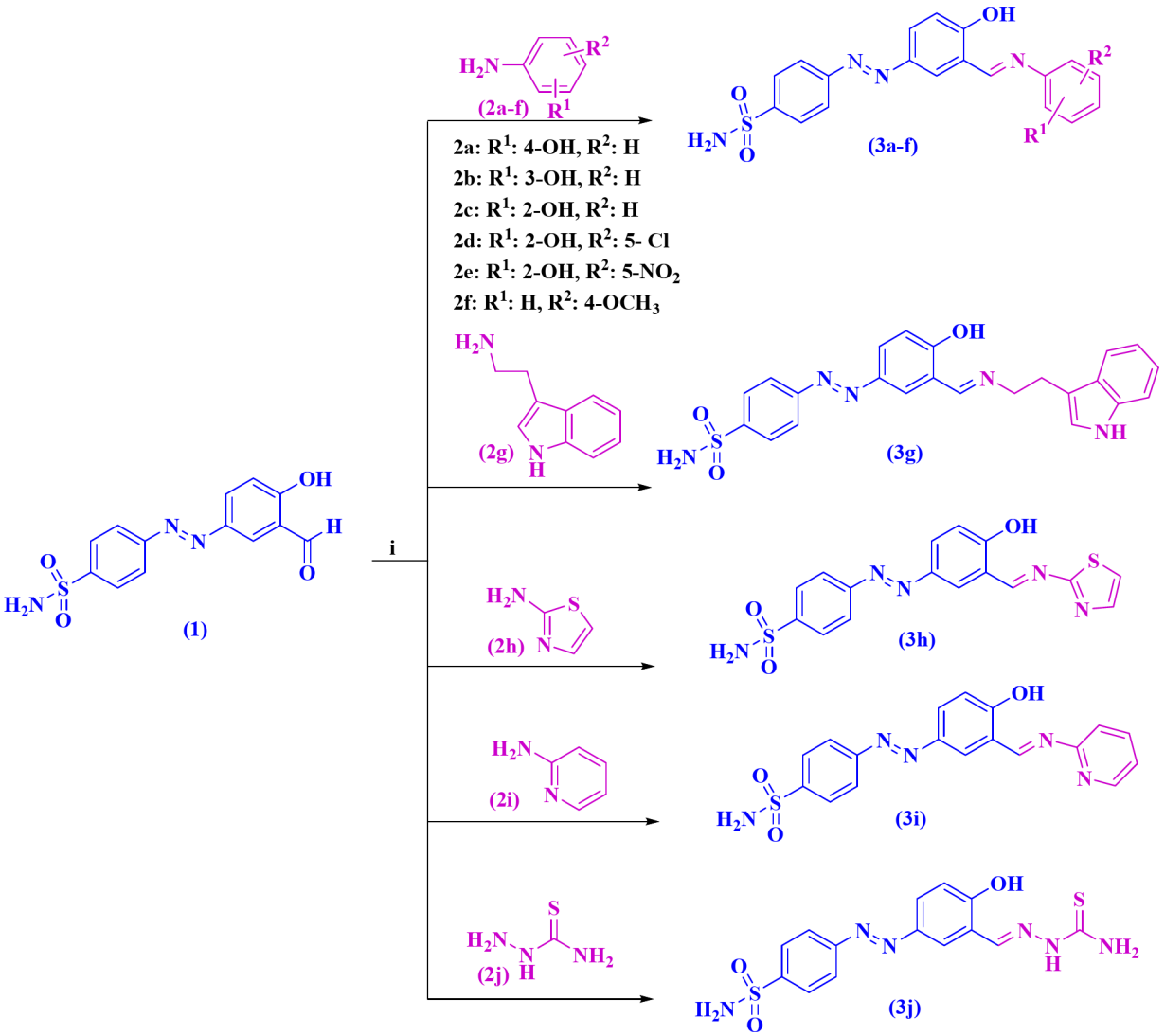

Fig. 3. Synthesis of sulfonamide-based Schiff base compounds **3a-j**. Reagents and conditions: (i) AcOH, MeOH, reflux, 4–5 h.

recorded on a Varian Gemini-200 (200 MHz, Foster City, Calif., USA), 300.1 and 100.13 spectrometers using dimethylsulphoxide DMSO-d_6 as a solvent and tetramethylsilane (TMS) as an internal standard (chemical shift in δ, ppm). High-resolution mass spectra (70 eV) were acquired using the Finnigan MAT 8430 mass spectrometer (Agilent 5975 C, Wilmington, DE).

*General procedure for Preparing schiff bases **3a-j***

A mixture of amine derivatives **2a-j** (2.25 mmol) and azo-based sulfonamide **1** (0.3 g, 2 mmol) in MeOH (20 mL) and five drops of acetic acid were added as a catalyst and heated under reflux for 4–5 h and the resulting precipitate was filtered, washed with cool EtOH/MeOH (1:1), and finally crystallized from EtOH to give pure product.

The structure of products was characterized using IR, ^{1}H, and ^{13}C NMR, and mass spectra. The spectral data of **3a** are reported below as an example, and the rest of the spectral data of other compounds (**3b-j**) have been given in the supplementary information.

*4-((E)-(4-hydroxy-3-((E)-((4-hydroxyphenyl)imino)methyl)phenyl)diazenyl)benzenesulfonamide (**3a**).*

Dark orange powder; Yield 86%; m.p. 285–287 °C. IR (KBr, cm^{-1}): 3417 (OH), 3314 (NH_2) 3059 (C_{sp2}–H), 1622 (C = N), 1599 (C = C), 1515 (N = N), 1336 (SO_2-asym), 1163 (SO_2-sym).

^{1}H NMR (300.1 MHz, DMSO-d_6): δ_H 6.89 (2 H, d, $^3J_{HH}$ =8.7 Hz, CH_{Ar}), 7.14 (1H, d, $^3J_{HH}$ = 8.7 Hz, CH_{Ar}), 7.41 (2 H, d, $^3J_{HH}$ = 8.7 Hz. CH_{Ar}), 7.54 (2 H, s, NH_2), 8.0-8.06 (m, 5 H, CH_{Ar}), 8.30 (1H, d, $^4J_{HH}$ = 2.7 Hz, CH_{Ar}), 9.13 (1H, s, HC = N), 9.82 (1H, s, OH), 14.50 (1H, s, OH) ppm.^{13}C NMR (100.13 MHz, DMSO-d_6): δ_C. 116. 5, 118.7, 119.7, 123.0, 123.3, 127.3, 127.5, 128.9, 138.4, 145.0, 145.7, 154.0, 157.8, 159.8, 165.4 ppm. MS: m/z (%): 396 ($M^{+\bullet}$, 14%), 212 [$M^{+\bullet}$-($N_2C_6H_4SO_2NH_2$), 28%], 172 [($H_2NC_6H_4SO_2NH_2$), 98%], 156 [$M^{+\bullet}$-($C_6H_4SO_2NH_2$), 100%].

Biological evaluation

Cytotoxicity assay

The anticancer effects of compounds **3a-j** were assessed using the standard MTT (3-(4,5-dimethylthiazol-2-yl)-2,5-diphenyltetrazolium bromide) assay on MCF-7 and MCF-10 A cell lines, which were obtained from the Pasteur Institute in Tehran, Iran.

To conduct cytotoxicity and antitumor tests, cell lines were placed in 96-well tissue culture plates with a cell density of 5 × 104 cells per well in media. After the 24 h incubation period, four different concentrations of compounds were added to the plates, with three repetitions. Control wells with only medium or 0.5% DMSO were also included. After another 24 h of incubation, the viability of the cells was determined using the MTT test. Then, the medium was carefully aspirated, and the formazan crystals were solubilized in 100 mL of DMSO for approximately 10 min. The absorbance of the suspension was measured at 570 nm using a spectrophotometer[37–39]. The inhibition percentage was calculated using the following formula:

% Inhibition = (Mean $abs_{control}$- Mean $abs_{compound}$)/Mean $abs_{control}$ 100%.

Statistical data analysis

To determine the IC_{50} values of the tested compounds **3a-j**, cells were treated with different concentrations of each compound. The data were subjected to analysis utilizing GraphPad Prism 9, and the findings were articulated as a mean ± standard deviation (SD) derived from three replicates. Statistical analyses were performed using two-way ANOVA followed by Tukey's multiple comparison test, and a P value of < 0.05 was obtained, which is deemed statistically significant[40].

Molecular docking studies

Molecular docking studies were conducted using the Schrödinger 9.6 Maestro software[41]. The focus of the study was to understand the binding mode of newly obtained compounds **3a-j** with the BRCA2 receptor (PDB ID: 3EU7) at the molecular level. To prepare the ligands for docking, LigPrep was utilized, and the ligands were sketched in 3D format using the build panel. The protein was primed using the protein preparation wizard by adding hydrogen atoms and removing the solvent, with further minimization performance. We utilized the co-crystallized bound ligand to generate grids for molecular docking. These grids were generated in the protein catalytic site and demonstrated that they occupy a comparable binding pocket with a root mean square deviation (RMSD) of 0.715 Å. This finding further strengthens the reliability of the docking protocol. Employing Glide extra-precision (XP) mode, compounds **3a-j** were docked, and three poses were saved for each molecule.

Molecular dynamics simulations

Molecular dynamics (MD) simulations were performed via the AMBER 22 software package with the ff99SB force field for proteins and the General Amber Force Field (GAFF) for ligands[42]. Partial charges for ligands were assigned via the Antechamber module in AmberTools, which employs the AM1-BCC method, which is consistent with established protocols[43]. Sodium ions (Na^+) were added to achieve a physiological salt concentration of 0.15 M. To avoid boundary artifacts, a minimum distance of 10 Å was maintained between solute molecules and the edges of the simulation box. Long-range electrostatic interactions were treated via the particle–mesh Ewald (PME) method[44], and covalent bonds involving hydrogen atoms were constrained via the SHAKE algorithm[45]. The system temperature was maintained at 310 K via a Langevin thermostat, with a time step of 2.0 fs for all MD simulations. The system underwent energy minimization (100,000 steps) followed by equilibration under NVT and NPT ensembles for 0.001 μs each. A production run of 0.5 μs was subsequently performed. Binding affinities were evaluated via a Python script to calculate implicit solvation binding energies via the Molecular Mechanics Generalized Born Surface Area (MM-GBSA) model[46,47].

Drug-likeness and in silico ADMET

The evaluation of the drug-like qualities of specific **3a-j** structures was conducted using Lipinski's rule of five (Ro5). Lipinski's Ro5 is widely employed as a filter to classify molecules according to their similarity to lead compounds, and it aids in determining the ability of compounds to be absorbed orally. In the current work, we utilized online tools like Swiss-ADME (accessible at http://www.swissadme.ch/index.php) to assess the dr ug-likeness and ADMET properties of the synthesized compounds. Swiss-ADME offers predictions on crucial aspects like physicochemical properties, drug-likeness, and medicinal chemistry compatibility. On the other hand, pkCSM provides predictive models for key ADME properties essential in drug development.

Antioxidant activity

Compounds **3a-j** were assessed for their ability to scavenge the 2,2-diphenyl-picrylhydrazyl (DPPH) free radical using spectrophotometry[48]. To start, a solution containing the products at a concentration of 1.0 mg/mL was prepared in DMSO. Then, 1.0 mL of each compound's solution was combined with 1.0 mL of DPPH solution (0.1 mM in MeOH) and incubated in the dark at RT for 60 min. The absorbance of the different solutions and the control DPPH was measured at 517 nm, and Eq. 1 was utilized to calculate the inhibition percentage of the DPPH radical scavenger.

$$\%\ \text{scavenging activity} = (\text{Abs of control} - \text{Abs of the sample}) / (\text{Abs of control}) \times 100 \quad (1)$$

Results and discussion

Chemistry

According to Fig. 3, condensation reactions between azo-based sulfonamide aldehyde **1** with various primary amines (**2a-j**) were carried out in MeOH under reflux conditions in the presence of acetic acid (as an acidic catalyst) that led to sulfonamide-based Schiff bases **3a-j** in high yields (75 to 89%).

The newly synthesized derivatives **3a-j** were characterized by spectroscopic data (IR, ^{1}H NMR, ^{13}C NMR), and MS spectra. The IR spectra of **3a-j** showed absorption bands ranging from 1607 to 1638 cm^{-1}, corresponding to the imine group. Their ^{1}H NMR spectra showed distinct protons of Schiff bases (N = CH) in the range of 8.46–9.66 ppm as singlet signals. Furthermore, their ^{13}C NMR spectra exhibited a signal in the range of 161.3–164.4 ppm for the carbon atoms of the N = CH group which confirms the desired structure.

The identification of compound **3a** is provided here as an example. Its IR spectrum revealed absorption bands at 3417 and 3314 cm^{-1} indicating the presence of the OH and NH_2 groups, respectively, and a band of medium intensity at 1622 cm^{-1}, which is attributed to the C = N group (stretching vibration). Furthermore, a sharp peak at 1515 cm^{-1} was identified for the N = N group, along with two absorption bands at 1336 and 1163 cm^{-1} attributed to the asymmetric and symmetric stretching of the SO_2 group.

The ^{1}H NMR spectrum of compound **3a** in DMSO-d6 revealed the presence of two singlet signals at δ 14.50 and 9.82 ppm, which are attributed to the two OH groups, a singlet at 9.13 ppm for the azomethine group, and a broad singlet at δ 7.54 ppm for the NH_2 group. Furthermore, the aromatic protons appeared in the appropriate regions. The ^{13}C NMR spectrum of compound **3a** displayed a signal at 165.45 ppm for the *C = N group and two signals at 157.80 and 159.83 ppm for the *C-O groups. The remaining signals at 154.03, 145.76, 145.03, 138.42, 128.90, 127.55, 127.34, 123.30, 123.08, 119.74, 118.77, and 116. 56 ppm are also attributed to its aromatic carbons. The mass spectrum acquired for compound **3a** exhibited molecular ion ($M^{+\bullet}$) and base peaks at *m/z* = 396 and 156, respectively. Additional peaks corresponded to fragment ions [M-($N_2C_6H_4SO_2NH_2$)] and [M-(OH + N = C-$C_6H_4SO_2NH_2$)] appeared at *m/z* = 212 and 196, respectively.

The structures of compounds **3b-j** have been confirmed using the reported spectral data in the supplementary information file.

Biological evaluation

In vitro anti-cancer activity

The cytotoxic impacts of compounds **1** and **3a-j** were evaluated against cell lines of MCF-7 and MCF-10 A through the MTT method after 48 and 72 h[49]. As presented in Table 1, compounds **3a-j** exhibited good to high anticancer activity (IC_{50} = 4.25 ± 0.009 to 9.49 ± 0.012 µM) against MCF-7 cell lines after 72 h. Also, the results in Figs. S48 and S49 in the supporting information display that when the concentration of compounds is increased, the anticancer activities are enhanced. Among them, compound **3i** exhibited the highest toxicity against MCF-7 cancer cell lines (IC_{50} = 4.25 ± 0.009 µM) and the lowest toxicity against MCF-10 A cell lines (IC_{50} = 48.73 ± 0.01 µM) after 72 h (entry 10).

Also, the selectivity index (SI) was calculated as the ratio of the IC_{50} for the MCF-10 A cell line to the IC_{50} for the MCF-7 cell line and is reported in Table 1. Among the tested compounds, **3i** displayed the highest selectivity index (SI) of 6.02 after 48 h and 11.46 after 72 h, whereas for doxorubicin it is 3.86 and 4.20, respectively. Although doxorubicin is more potent against MCF-7 cells with an IC_{50} value of (0.68 ± 0.100 µM) after 72 h, its SI (4.20) is lower than compound **3i**. These results indicate that compound **3i** could be a promising candidate for further medical trials in breast cancer treatment studies.

Structure-activity relationship studies (SAR)

As seen in Table 1, among the synthesized Schiff bases from the aminophenols (**3a-c**), compound **3b** containing a phenolic OH group at the *meta*-position has the highest cytotoxicity (IC_{50} = 6.69 ± 0.001 µM) compared to *ortho*- and *para* derivatives (IC_{50} = 9.26 ± 0.002 and 9.49 ± 0.012 µM, respectively)[50,51]. While the Schiff bases with a phenolic OH group at *ortho*-position and an electron-withdrawing substituent such as Cl or NO_2 (**3d** and **3e**) exhibited higher cytotoxicity (IC_{50} = 5.00 ± 0.004 and 8.23 ± 0.004 µM, respectively) than compound

		IC^{b}_{50} ±SD[a] (μM)					
		MCF-7		MCF-10 A		Selectivity Index (SI)	
Entry	Compounds	48 h	72 h	48 h	72 h	48 h	72 h
1	**1**	8.44 ± 0.009	9.15 ± 0.006	18.72 ± 0.010	31.84 ± 0.008	2.21	3.47
2	**3a**	10.90 ± 0.005	9.49 ± 0.012	11.18 ± 0.012	1.98 ± 0.002	1.02	0.20
3	**3b**	25.43 ± 0.007	6.69 ± 0.001	20.92 ± 0.010	9.63 ± 0.001	0.82	1.43
4	**3c**	21.16 ± 0.014	9.26 ± 0.002	16.82 ± 0.010	2.23 ± 0.001	0.79	0.24
5	**3d**	5.07 ± 0.012	5.00 ± 0.004	12.17 ± 0.010	8.75 ± 0.014	2.40	1.75
6	**3e**	9.28 ± 0.010	8.23 ± 0.004	13.90 ± 0.016	4.42 ± 0.006	1.49	0.53
7	**3f**	8.94 ± 0.013	7.62 ± 0.018	11.01 ± 0.016	2.67 ± 0.009	1.23	0.35
8	**3 g**	9.02 ± 0.022	5.89 ± 0.002	10.46 ± 0.006	16.42 ± 0.080	1.15	2.78
9	**3 h**	9.22 ± 0.010	6.82 ± 0.002	34.69 ± 0.010	13.11 ± 0.007	3.76	1.92
10	**3i**	4.85 ± 0.006	4.25 ± 0.009	29.22 ± 0.009	48.73 ± 0.010	6.02	11.46
11	**3j**	6.52 ± 0.007	5.27 ± 0.006	17.43 ± 0.019	11.26 ± 0.008	2.67	2.13
12	Doxorubicin	3.42 ± 0.100	0.68 ± 0.100	13.20 ± 0.100	2.85 ± 0.100	3.86	4.20

Table 1. Anticancer activities of compounds **1** and **3a-j** against MCF-7 and MCF-10 A cell lines after 48 and 72 h. [a] SD is the standard deviation. [b] IC_{50} values are reported as the mean ± SD from a minimum of three independent experiments, ($p < 0.05$)

Compound	MW	Log *p*	nHBA	nHBD	nRot	TPSA	Bioavailability Score	Lipinski's violations
3a	396.42	2.72	8	3	5	146.08	0.55	0
3b	396.42	2.81	8	3	5	146.08	0.55	0
3c	396.42	2.91	8	3	5	146.08	0.55	0
3d	430.86	3.36	8	3	5	146.08	0.55	0
3e	441.42	2.26	10	3	6	191.90	0.55	1
3f	410.45	3.23	8	2	6	135.08	0.55	0
3 g	378.43	1.39	7	4	6	195.99	0.55	0
3 h	447.51	3.60	7	3	7	141.64	0.55	0
3i	387.44	2.67	8	2	5	166.98	0.55	0
3j	381.41	2.68	8	2	5	138.74	0.55	0
Dox	543.52	0.44	12	5	6	206.07	0.17	3

Table 2. In Silico ADME prediction of compounds **3a-j**.

3c (IC_{50} = 9.26 ± 0.002 μM), against MCF-7 cell line. It seems that electron-withdrawing substituents play an important role in their anticancer activity[52]. When OMe was replaced instead of OH in compound **3f** (IC_{50} = 7.62 ± 0.018 μM), the cytotoxicity was increased against MCF-7, compared to **3a**[53]. Likewise, compounds **3 g**, **3 h**, and **3i**, containing heterocyclic moieties such as indole, thiazole, and pyridine displayed good anticancer activity (IC_{50} = 5.89 ± 0.002, 6.82 ± 0.002, and 4.25 ± 0.009 μM, respectively) against cancer cell lines (Table 1)[54–57]. Similarly, the thiosemicarbazone derivative **3j** demonstrated significant anticancer efficacy against the MCF-7 cell lines (IC_{50} = 5.27 ± 0.006)[58]. Most compounds exhibit significant cytotoxicity against the MCF-10 A cell lines. However, compound **3i** showed the highest cytotoxicity against the MCF-7 and the least toxicity against MCF-10 A (IC_{50} = 48.73 ± 0.**010** μM).

To better understand how synthesized compounds interact with gene-active sites, in silico studies were conducted.

In Silico ADME prediction and drug-likeness study

To assess the potential of the studied molecules as drug candidates, their pharmacokinetic profiles, drug-likeness, and bioavailability were analyzed using Swiss-ADME[59].

We have assessed the drug-like qualities of the synthesized compounds based on Lipinski's rule of 5 (Table 2). The molecular weights of these compounds are between 378.43 and 447.51 g/mol, which fall within the allowed range (< 500) for easy transport, absorption, and diffusion in the body. Furthermore, the Log Pw/o values (the octanol/water partition coefficient) of the compounds were calculated at 1.39 to 3.60, which are in the acceptable ranges (< 4). The obtained values of H-bond acceptors and donors for the compounds (≤ 10 and ≤ 5, respectively), and values of rotatable bonds (≤ 10), consist of the allowed values in Lipinski's rule. Most of the analyzed compounds have a topological polar surface area (TPSA) of less than 160 $Å^2$, indicating good solubility,

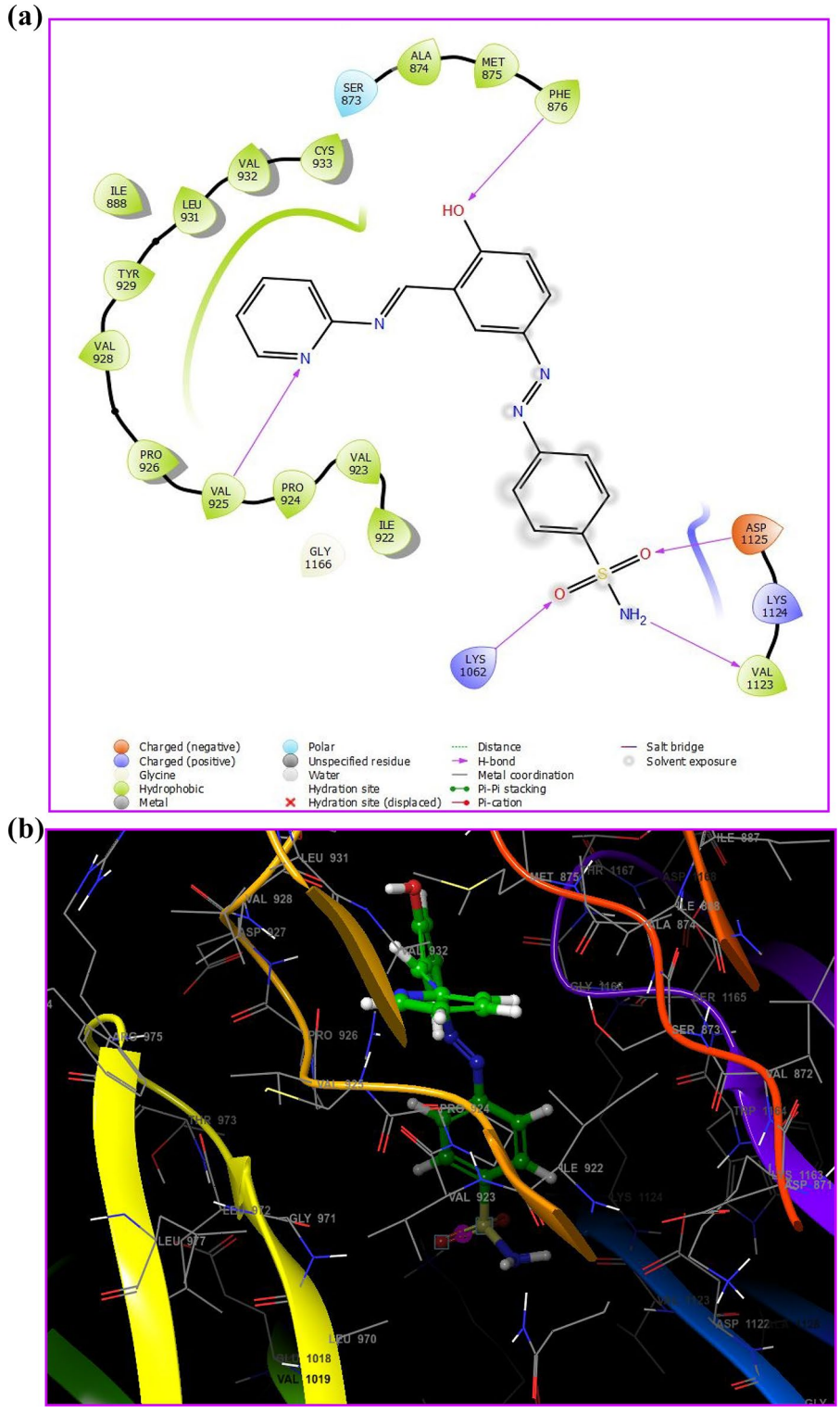

Fig. 4. 2D binding interactions of **3i** with the active pocket of BRCA2. 3D binding interactions of **3i** with the active pocket of BRCA2

cell membrane penetration, and intestinal absorption. Since these compounds can be effectively transported in the intestines, they can be good candidates for drug transport.

Furthermore, the obtained bioavailability score of all compounds within the recommended range (0.55), indicates that they can be easily absorbed and metabolized by the body and exhibit pharmaceutical activity.

Compound	Docking score (kcal/mol)	Amino acids	Interacting groups	Type of interaction	Structural formula
3a	-6.44	GLN (921)	S=O	H-bond acceptor	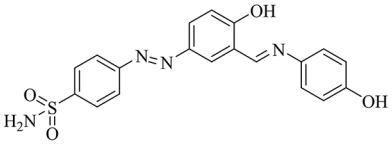
		LYS (1163)	Phenyl	cation-π	
		TRP (1164)	OH	H-bond donor	
		ASP (927)	OH	H-bond acceptor	
3b	-7.04	VAL (1123)	NH_2	H-bond donor	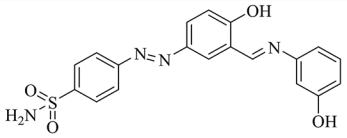
		ASP (1125)	S=O	H-bond acceptor	
		PHE (876)	OH	H-bond acceptor	
		CYS (933)	OH	H-bond acceptor	
3c	-6.56	VAL (1123)	NH_2	H-bond donor	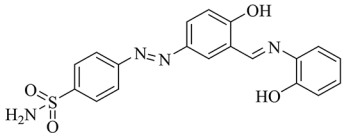
		LYS (1062)	S=O	H-bond acceptor	
		PHE (876)	OH	H-bond acceptor	
3d	-6.45	VAL (969)	NH_2	H-bond donor	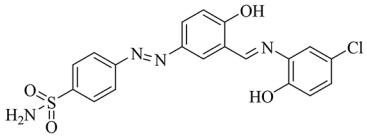
		PHE (1016)	S=O	H-bond acceptor	
		TRP (1164)	OH	H-bond donor	
3e	-5.96	VAL (925)	NH_2	H-bond donor	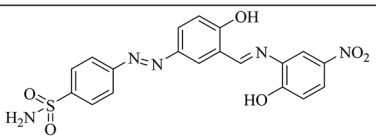
		ASP (927)	S=O	H-bond acceptor	
		PHE (876)	S=O	H-bond acceptor	
		VAL (1123)	OH	H-bond donor	
		ASP (1125)	OH	H-bond acceptor	
		LYS (1062)	OH	Salt bridges	
3f	-6.50	PHE (1016)	NH_2	H-bond donor	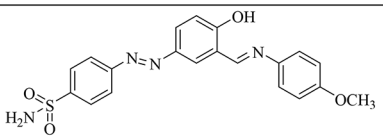
		VAL (969)	NH_2	H-bond donor	
		TRP (1164)	OH	H-bond donor	
		ASP (927)	OCH_3	H-bond acceptor	
		GLN (921)	NH_2	H-bond donor	
		VAL (969)	NH_2	H-bond donor	

Table 3. Molecular Docking scores for sulfonamide-based schiff bases **3a-j** at the active sites of the BRCA2 receptor.

Docking study

According to the results of anticancer activities of the synthesized compounds, docking studies were performed to predict binding interactions between the compounds **3a-j** and the BRCA2 enzyme (PDB: 3EU7) as a receptor. The results in Table 3 display that the compounds were stabilized by the formation of hydrogen bonding between the ligand's core structure and residue amino acids of the receptor's active site. Among them, the compound **3i** shows the highest binding affinity at -7.99 kcal/mol. The suggested binding position of compound **3i** in conjunction with BRCA2 shows five significant hydrogen bonds, a hydrogen bond between the phenolic OH

3g	-6.11	PHE (1016)	S=O	H-bond acceptor	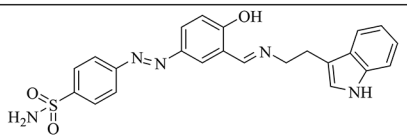
		TRP (1164)	OH	H-bond donor	
		ASP (1122)	C=N	Salt bridges	
		HIE (1061)	NH	H-bond donor	
		LYS (1062)	Phenyl	cation-π	
		LYS (1062	Pyrrole	cation-π	
3h	-5.68	VAL (969)	NH_2	H-bond donor	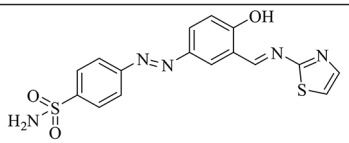
		PHE (1016)	S=O	H-bond acceptor	
		TRP (1164)	OH	H-bond donor	
3i	-7.99	VAL (1123)	NH_2	H-bond donor	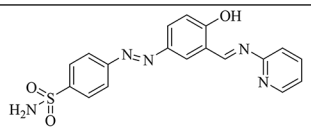
		ASP (1125)	S=O	H-bond acceptor	
		LYS (1062)	S=O	H-bond acceptor	
		PHE (876)	OH	H-bond acceptor	
		VAL (925)	N-pyridine	H-bond acceptor	
3j	-6.63	VAL (925)	NH_2	H-bond donor	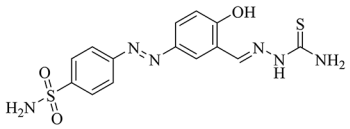
		PHE (876)	S=O	H-bond acceptor	
		VAL (928)	S=O	H-bond acceptor	
		LYS (1062)	OH	Salt bridges	
		ASP (1125)	OH	H-bond acceptor	
		LYS (1062)	OH	H-bond acceptor	
		HIE (1061)	NH	H-bond donor	
		GLU (1018)	C=S	H-bond acceptor	
		HIE (1061)	NH_2	H-bond donor	
1	-6.28	VAL (1123)	NH_2	H-bond donor	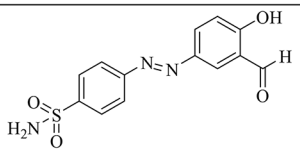
		ASP (1125)	S=O	H-bond acceptor	
		PHE (876)	OH	H-bond acceptor	
		VAL (925)	C=O	H-bond acceptor	
Doxorubicin	-6.79	LYS (1163)	C=O	H-bond acceptor	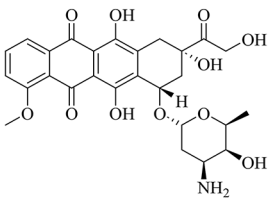
		ASP (1122)	NH_2	Salt bridges	
		PHE (1016)	C=O	H-bond acceptor	
		PHE (1016)	OH	H-bond donor	
		VAL (969)	OH	H-bond donor	

Figure 3. (continued)

group and the PHE 87 amino acid residue, a hydrogen bond between the NH_2 group and the amino acid VAL 1123, a hydrogen-bond between *N*-atom of pyridine ring and VAL 925 as well as two hydrogen bonds between the two S = O groups with ASP 1125 and LYS 1062 amino acid residues (Fig. 4A and B).

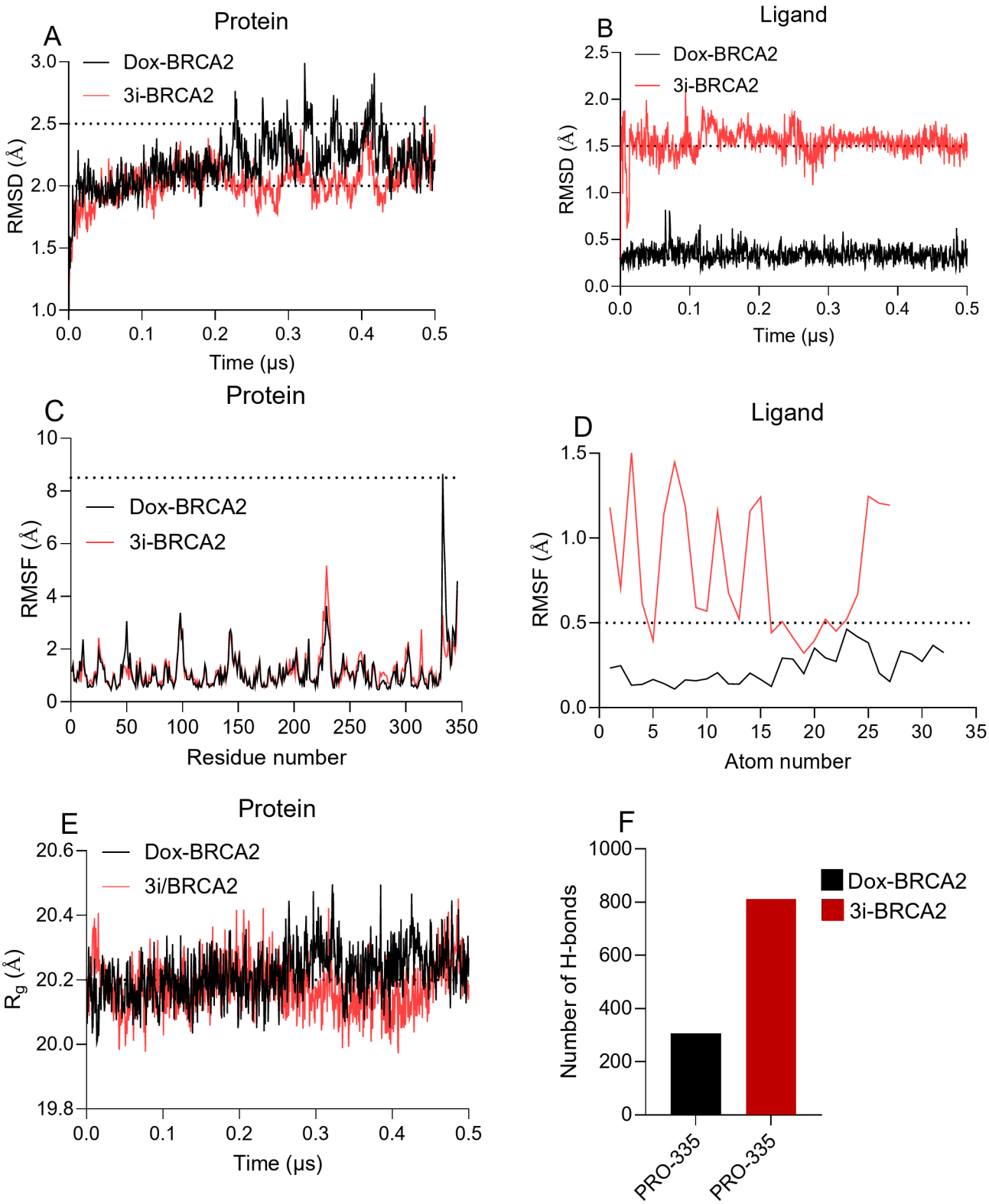

Fig. 5. MD simulation analyses of the DOX-BRCA2 and **3i**-BRCA2 complexes. (A, B) Root-mean-square deviation (RMSD) profiles over time for DOX-BRCA2 and **3i**-BRCA2, respectively. (C, D) Root-mean-square fluctuation (RMSF) profiles for the same complexes. (E) The radius of gyration (Rg) of the complexes throughout the simulation. (F) The number of hydrogen bonds (H-bonds) formed between the.

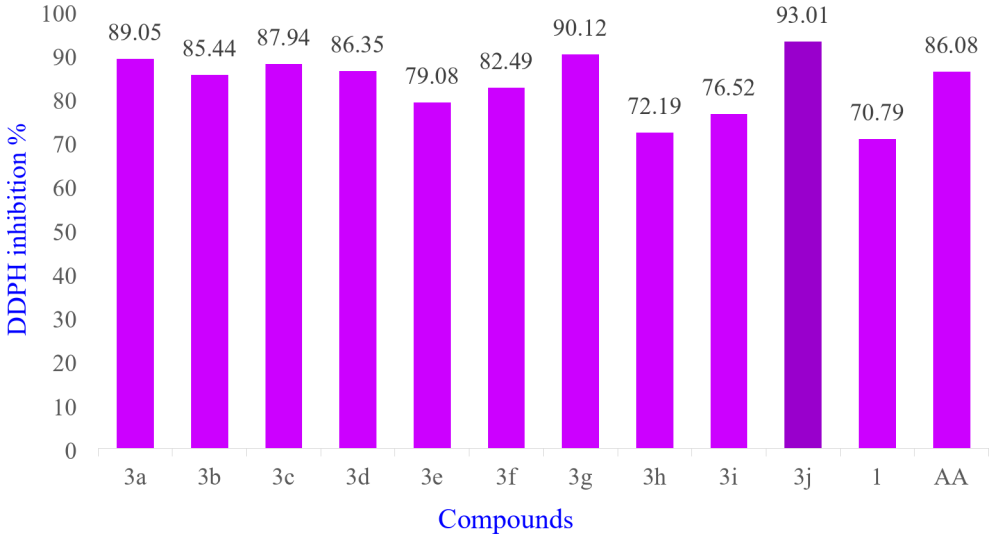

Fig. 6. Antioxidant activity of the synthesized compounds **1** and **3a-j**.

Energy Term	Average		Std. Dev.	
	DOX-BRCA2	3i-BRCA2	DOX-BRCA2	3i-BRCA2
E_{vdw}	-12.89	-24.99	4.59	7.92
E_{el}	-14.01	-11.85	15.41	9.45
E_{gb}	21.37	27.78	16.34	9.3
E_{surf}	-1.81	-3.68	0.5	0.99
ΔG_{gas}	-26.9	-36.85	15.86	11.93
ΔG_{solv}	19.55	24.09	16.15	8.88
ΔG_{tot}	-7.35	-12.75	4.16	5.05

Table 4. Binding energy values (kcal/mol) for the protein-ligand complexes predicted via the MM-GBSA method. Abbreviations: Evdw–van der Waals energy; Eel–electrostatic energy; Egb–MM-GBSA polar solvation energy; Esurf–MM-GBSA nonpolar solvation energy; ΔGgas–net gas phase energy; ΔGsolv–net solvation energy; ΔGtot–net system energy.

These results demonstrate that the **3i** molecule can serve as a novel inhibitor of BRCA2 gene functions, potentially aiding in the creation of more effective drugs for treating breast cancer.

Molecular dynamics simulations

To validate the molecular docking results and investigate the dynamic behavior of the ligand-protein complexes within a lipid membrane environment, molecular dynamics (MD) simulations were conducted (Fig. 5). The receptor's root-mean-square deviation (RMSD) for both the DOX–BRCA2 and **3i**–BRCA2 complexes remained stable within a range of 2.0–2.5 Å (Fig. 5A). Conversely, the ligands DOX and **3i** presented lower RMSD values, remaining below 2.0 Å. DOX demonstrated a minimal deviation of approximately 0.3 Å, whereas **3i** deviated by approximately 1.5 Å from its initial conformation (Fig. 5B).

Analysis of the receptor's root-mean-square fluctuation (RMSF) revealed significant flexibility, with an RMSF of approximately 8.5 Å in the BRCA2 peptide segment of the PALB2/BRCA2 complex (Fig. 5C). Ligand RMSF data indicated greater atomic fluctuations for **3i** (exceeding 0.5 Å) than for DOX (below 0.5 Å) (Fig. 5D). The radius of gyration (Rg) for both complexes was consistent at approximately 20.2 Å, suggesting minimal changes in protein compactness upon ligand binding (Fig. 5E).

Hydrogen bond analysis revealed a greater number of hydrogen bonds in the **3i**–BRCA2 complex, with Pro-335 emerging as a key residue contributing significantly to these interactions (Fig. 5F). Furthermore, binding free energy calculations via the MM-GBSA method during 0.5 μs MD simulation (Table 4) reinforced these findings, confirming a stronger binding affinity of **3i** for BRCA2 than for the reference molecule (DOX).

key amino acid residue—the residue forming the maximal number of H-bonds during the MD simulation—and the ligand during 0.5 μs for the DOX and **3i** ligands bound to BRCA2. Threshold values are indicated by dotted lines.

Entry	Compounds	$IC_{50} \pm SD$ (μM)
1	**3a**	13.16 ± 0.74
2	**3b**	13.98 ± 1.22
3	**3c**	13.55 ± 0.95
4	**3d**	13.68 ± 1.56
5	**3e**	14.34 ± 0.63
6	**3f**	14.04 ± 1.45
7	**3 g**	13.05 ± 0.86
8	**3 h**	16.37 ± 0.33
9	**3i**	15.24 ± 1.77
10	**3j**	12.36 ± 0.55
11	**1**	16.99 ± 0.43
12	**AA**	13.58 ± 0.38

Table 5. The DPPH radical scavenging ability of compounds **1** and **3a-j**.

Antioxidant activity

The in vitro antioxidant activity of sulfonamide-based Schiff bases **1** and **3a-j** was assessed using the DPPH radical scavenging method developed by Blois[60]. Antioxidants with a high number of heteroatoms, π-electrons, and exchangeable hydrogen atoms are more efficient at neutralizing the free radicals generated by DPPH. A decrease in absorption at a wavelength of 517 nm may suggest the existence of antioxidants, as evidenced by a color change in the DPPH test solution from dark purple to light yellow. Figure 5 demonstrates that the synthesized Schiff bases in this work **3a-i** effectively inhibited DPPH with potencies of 72.19–93.01%. Moreover, the antioxidant properties of compounds **1** and **3a-j** were assessed by determining their IC_{50} values. The results indicated that the antioxidant activity of tested molecules is comparable with ascorbic acid as a standard antioxidant (Table 5; Fig. 6). The observed high antioxidant activity of the sulfonamide-based Schiff bases could be due to the existence of exchangeable protons (NH_2 and OH groups), several heteroatoms (oxygen, nitrogen, and sulfur atoms), and π-electrons (C = N, N = N, and aromatic rings) in their structures.

Conclusion

In this study, the target sulfonamide-based Schiff bases **3a-j** were effectively synthesized, and assessed their effects on MCF-7 and MCF-10 A cell lines. In addition, all compounds demonstrated good to excellent activity against MCF-7 cancer cell lines and also displayed significant antioxidant activities comparable with the standard ascorbic acid. Interestingly, compound **3i** exhibited as the most potent compound against MCF-7, $IC_{50} = 4.85 \pm 0.006$ and 4.25 ± 0.009 μM at 48 and 72 h, respectively. The molecular docking results showed that the most effective anticancer compound would be compound **3i** with a docking score of -7.99 kcal/mol. This might be because of the existence of hydrogen acceptors in its structure, which resulted in strong hydrogen bond interactions with the key amino acids of the related protein BRCA2. Compound **3i** showed the least activity against MCF-10 A cell lines, which could set the stage for further research and development as a potential agent for the treatment of breast and other types of cancers. The MD simulations of the **3i**-BRCA2 and DOX-BRCA2 complexes exhibited a stronger binding affinity for **3i** than DOX, which could make it a more effective ligand for targeting BRCA2 in therapeutic applications. The experimental data correlated well with the computational molecular docking analysis and in silico ADMET and Drug-Likeness findings. We hope the results of this study could potentially contribute to the development of new therapeutic agents in helpful fighting caused by breast cancer.

Data availability

The datasets utilized and/or analyzed in this study can be obtained from the manuscript and supplementary information files.

Received: 18 October 2024; Accepted: 18 February 2025
Published online: 24 February 2025

References

1. Rakha, E. A., Tse, G. M. & Quinn, C. M. An update on the pathological classification of breast cancer. *Histopathology* **82**, 5–16. https://doi.org/10.1111/his.14786 (2023).
2. Bray, F. et al. Global cancer statistics 2022: GLOBOCAN estimates of incidence and mortality worldwide for 36 cancers in 185 countries. *CA Cancer J. Clin.* **74**, 229–263. https://doi.org/10.3322/caac.21834 (2024).
3. Siegel, R. L., Miller, K. D., Fuchs, H. E. & Jemal, A. Cancer statistics, 2022. *CA Cancer J. Clin.* **72**, 7–33. https://doi.org/10.3322/caac.21708 (2022).
4. Chen, W., Hoffmann, A. D., Liu, H. & Liu, X. Organotropism: new insights into molecular mechanisms of breast cancer metastasis. *NPJ Precis Oncol.* **2**, 4. https://doi.org/10.1038/s41698-018-0047-0 (2018).
5. Anand, U. et al. Cancer chemotherapy and beyond: current status, drug candidates, associated risks and progress in targeted therapeutics. *Genes Dis.* **10**, 1367–1401. https://doi.org/10.1016/j.gendis.2022.02.007 (2023).
6. Kitta, A. The silent transition from curative to palliative treatment: a qualitative study about cancer patients' perceptions of end-of-life discussions with oncologists. *Support Care Cancer.* **29**, 2405–2413. https://doi.org/10.1007/s00520-020-05750-0 (2021).

7. Schnipper, L. E. et al. American society of clinical oncology statement: A conceptual framework to assess the value of Cancer treatment options. *J. Clin. Oncol.* **33**, 23. https://doi.org/10.1200/JCO.2015.61.6706 (2015).
8. Zhong, L. et al. Small molecules in targeted cancer therapy: advances, challenges, and future perspectives. *Signal. Transduct. Target. Ther.* **6**, 201. https://doi.org/10.1038/s41392-021-00572-w (2021).
9. Weth, F. R. et al. Unlocking hidden potential: advancements, approaches, and Obstacles in repurposing drugs for cancer therapy. *Br. J. Cancer*. **130**, 703–715. https://doi.org/10.1038/s41416-023-02502-9 (2024).
10. Apostolou, P. & Fostira, F. Hereditary breast cancer: the era of new susceptibility gene. *Biomed. Res. Int.* **2013** (747318). https://doi.org/10.1155/2013/747318 (2013).
11. Li, S. et al. ACancer risks associated with BRCA1 and BRCA2 pathogenic variants. *J. Clin. Oncol.* **40**, 1529–1541. https://doi.org/10.1200/JCO.21.02112 (2022).
12. Bishoyi, A. K., Mahapatra, M., Sahoo, C. R., Paidesetty, S. K. & Padhy, R. N. Design, molecular Docking and antimicrobial assessment of newly synthesized p-cuminal-sulfonamide schiff base derivatives. *J. Mol. Struct.* **1250**, 131824. https://doi.org/10.1016/j.molstruc.2021.131824 (2022).
13. Chalkha, M. A. et al. Crystallographic study, biological assessment and POM/Docking studies of pyrazoles-sulfonamide hybrids (PSH): identification of a combined antibacterial/antiviral pharmacophore sites leading to in-silico screening the anti-Covid-19 activity. *J. Mol. Struct.* **1267**, 133605. https://doi.org/10.1016/j.molstruc.2022.133605 (2022).
14. Ayoup, M. S. et al. Novel sulfonamide derivatives as multitarget antidiabetic agents: design, synthesis, and biological evaluation. *RSC Adv.* **14**, 7664–7675. https://doi.org/10.1039/d4ra01060d (2024).
15. Gaddi, G. M. et al. Phosphatase alkaline Inhibition and antithyroid activity of acetylacetone sulfonamide derived schiff base. In vitro and In Silico studies. *ChemistrySelect* **9**, e202401342. https://doi.org/10.1002/slct.202401342 (2024).
16. Abdel-Aziz, A. A. M. et al. Synthesis and anti-inflammatory activity of sulphonamides and carboxygenase/carbonic anhydrase inhibitory actions. *Bioorg. Chem.* **84**, 260. https://doi.org/10.1016/j.bioorg.2018.11.033 (2019).
17. Ukrainets, I. V., Bereznyakova, N. L. & Heterocyclic diuretics *Heterocycl. Chem.* **48**, 155–165. https://doi.org/10.1007/s10593-012-0979-1 (2012).
18. Rezaeianzadeh, O. et al. Molecular docking, and anticancer evaluation of new Azo-Based sulfonamides against MCF-7 human breast Cancer cell line. *Chem. Methodol.* **8**, 329–350. https://doi.org/10.48309/CHEMM.2024.447205.1773 (2024).
19. Kirane, A. et al. Apricoxib, a novel inhibitor of COX-2, markedly improves standard therapy response in molecularly defined models of pancreatic Cancer. *Clin. Cancer Res.* **18**, 5031–5042. https://doi.org/10.1158/1078-0432.CCR-12-0453 (2012).
20. Muccino, D. & Green, S. Update on the clinical development of gefapixant, a P2X3 receptor antagonist for the treatment of refractory chronic cough. *Pulm Pharmacol. Ther.* **56**, 75–78. https://doi.org/10.1016/j.pupt.2019.03.006 (2019).
21. Nijhuis, A. et al. Indisulam targets RNA splicing and metabolism to serve as a therapeutic strategy for high-risk neuroblastoma. *Nat. Commun.* **13**, 1380. https://doi.org/10.1038/s41467-022-28907-3 (2022).
22. McDonald, P. C. et al. A phase 1 study of SLC-0111, a novel inhibitor of carbonic anhydrase IX, in patients with advanced solid tumors. *Am. J. Clin. Oncol.* **43**, 484–490. https://doi.org/10.1097/COC.0000000000000691 (2020).
23. Palmieri, C., Januszewski, A., Stanway, S. & Coombes, R. C. Irosustat: a first-generation steroid sulfatase inhibitor in breast cancer. *Expert Rev. Anticancer Ther.* **11**, 179–183. https://doi.org/10.1586/era.10.201 (2011).
24. Mboge, M. Y. Inhibition of carbonic anhydrase using SLC-149: support for a Non-catalytic function of CAIX in breast Cancer. *J. Med. Chem.* **64**, 1713–1724. https://doi.org/10.1021/acs.jmedchem.0c02077 (2021).
25. Swain, B. et al. Design, synthesis, and biological evaluation of 3-benzenesulfonamide-linked 3-hydrazinoisatin derivatives as carbonic anhydrase inhibitors. *Arch. Pharm.* **357**, 2300718. https://doi.org/10.1002/ardp.202300718 (2024).
26. Gamal, M. A. et al. Probing benzenesulfonamide–thiazolidinone hybrids as multitarget directed ligands for efficient control of type 2 diabetes mellitus through targeting the enzymes: α-glucosidase and carbonic anhydrase II. *Eur. J. Med. Chem.* **271**, 116434. https://doi.org/10.1016/j.ejmech.2024.116434 (2024).
27. Harpstrite, S. E., Collins, S. D., Oksman, A., Goldberg, D. E. & Sharma, V. Synthesis, characterization, and antimalarial activity of novel schiff-base-phenol and naphthalene-amine ligands. *Med. Chem.* **4**, 392–395. https://doi.org/10.2174/157340608784872280 (2008).
28. Shaldam, M. A. et al. Novel sulfonamide-tethered schiff bases as anti-proliferative agents with VEGFR-2 inhibitory activity: synthesis, biological assessment, and molecular dynamic simulations. *J. Mol. Struct.* **1309**, 138148. https://doi.org/10.1016/j.molstruc.2024.138148 (2024).
29. Alafeefy, A. M. et al. Synthesis, analgesic, anti-inflammatory, and anti-ulcerogenic activities of certain novel Schiff's bases as Fenamate isosteres. *Bioorg. Med. Chem. Lett.* **25**, 179–183. https://doi.org/10.1016/j.bmcl.2014.11.088 (2015).
30. Ünlü, A. et al. Biological evaluation of schiff bases containing dopamine as antibacterial/antifungal and potential anti COVID-19 agents: design, synthesis, characterization, molecular Docking studies, and ADME properties. *J. Mol. Struct.* **1293**, 136318. https://doi.org/10.1016/j.molstruc.2023.136318 (2023).
31. Ceramella, J. et al. A review on the antimicrobial activity of schiff bases: data collection and recent studies. *Antibiotics* **13**, 423. https://doi.org/10.3390/antibiotics13050423 (2024).
32. Mahmoodi, N. O., Khalili, B., Rezaeianzadeh, O. & Ghavidast, A. One-pot multicomponent synthesis of indol-3-yl-hydrazinyl thiazoles as antimicrobial agents. *Res. Chem. Intermed.* **42**, 6531–6542. https://doi.org/10.1007/s11164-016-2478-y (2016).
33. Sriraman, V. et al. Synthesis, crystal structure, DFT, docking, and biological activity studies of (NZ,N'Z)-3,3'-(piperazine-1,4-diyl) bis(N-(-4-methyl benzylidene) propane-1-amine. *Mater. Chem. Phys.* **275**, 125220. https://doi.org/10.1016/j.matchemphys.2021.125220 (2022).
34. Ghorab, M. M. et al. Anticancer and radiosensitizing evaluation of some new pyranothiazole-Schiff bases bearing the biologically active sulfonamide moiety. *Eur. J. Med. Chem.* **53**, 403–407. https://doi.org/10.1016/j.ejmech.2012.04.009 (2012).
35. Eldehna, W. M. et al. Novel 4/3-((4-oxo-5-(2-oxoindolin-3-ylidene)thiazolidin-2-ylidene)amino) benzenesulfonamides: synthesis, carbonic anhydrase inhibitory activity, anticancer activity, and molecular modeling studies. *Eur. J. Med. Chem.* **139**, 250–262. https://doi.org/10.1016/j.ejmech.2017.07.073 (2017).
36. El-Malah, A. et al. Schiff bases as linker in the development of quinoline-sulfonamide hybrids as selective cancer-associated carbonic anhydrase isoforms IX/XII inhibitors: A new regio-isomerism tactic. *Bioinorg. Chem.* **131**, 106309. https://doi.org/10.1016/j.bioorg.2022.106309 (2023).
37. Senol, H., Aggül, A. G., Atasoy, S. & Güzeldemirci, N. Synthesis, characterization, molecular docking and in vitro anti-cancer activity studies of new and highly selective 1,2,3-triazole substituted 4-hydroxybenzohyrdazide derivatives. *J. Mol. Struct*. 1283, 135247. (2023). https://doi.org/10.1016/j.molstruc. 135247 (2023).
38. Senol, H., Aggül, A. G., Atasoy, S. & Synthesis Characterization, molecular Docking and in vitro biological studies of Thiazolidin-4-one derivatives as Anti-Breast-Cancer agents. *ChemistrySelect* **8**, e202300481. https://doi.org/10.1002/slct.202300481 (2023).
39. Demirkıran, Ö. et al. Cytotoxic meroterpenoids from brown Alga Stypopodium schimperi (Kützing) verlaque & Boudouresque with comprehensive molecular Docking & dynamics and ADME studies. *Process. Biochem.* **136**, 90–108. https://doi.org/10.1016/j.procbio.2023.11.029 (2024).
40. Tokali, F. S., Senol, H., Bulut, S. & Haciosmanoglu-Aldogan, E. Synthesis, characterization and molecular Docking studies of highly selective new hydrazone derivatives of anthranilic acid and their ring closure analog Quinazolin-4(3H)-ones against lung cancer cells A549. *J. Mol. Struct.* **1282**, 135176. https://doi.org/10.1016/j.molstruc.2023.135176 (2023).

41. Vanitha, U., Elancheran, R., Manikandan, V., Kabilan, S. & Krishnasamy, K. Design, synthesis, characterization, molecular Docking and computational studies of 3-phenyl-2-thioxoimidazolidin-4-one derivatives. *J. Mol. Struct.* **1246**, 13121. https://doi.org/10.1016/j.molstruc.2021.131212 (2021).
42. Case, D. A. et al. The amber biomolecular simulation programs. *J. Comput. Chem.* **26**, 1668–1688. https://doi.org/10.1002/jcc.20290 (2005).
43. Marques, S. M. et al. Screening of natural compounds as P-glycoprotein inhibitors against multidrug resistance. *Biomedicines* **9**, 357. https://doi.org/10.3390/biomedicines9040357 (2021).
44. Essmann, U. et al. A smooth particle mesh Ewald method. *J. Chem. Phys.* **103**, 8577–8593. https://doi.org/10.1063/1.470117 (1995).
45. Miyamoto, S., Kollman, P. A. & Settle An analytical version of the SHAKE and RATTLE algorithm for rigid water models. *J. Comput. Chem.* **13**, 952–962. https://doi.org/10.1002/jcc.540130805 (1992).
46. Shityakov, S. et al. Scaffold searching of FDA and EMA-approved drugs identifies lead candidates for drug repurposing in Alzheimer's disease. *Front. Chem.* **9**, 736509. https://doi.org/10.3389/fchem.2021.736509 (2021).
47. Khalid, H. & Shityakov, S. Immunoinformatics-driven design and computational analysis of a multiepitope vaccine targeting uropathogenic Escherichia coli. *Silico Pharmacol.* **13**, 2. https://doi.org/10.1007/s40203-024-00288-z (2025).
48. Anitha, S., Krishnan, S., Senthilkumar, K. & Sasirekha, V. A comparative investigation on the scavenging of 2,2-diphenyl-1-picrylhydrazyl radical by the natural antioxidants (+) Catechin and (-) epicatechin. *J. Mol. Struct.* **1242**, 130805. https://doi.org/10.1016/j.molstruc.2021.130805 (2021).
49. He, C. et al. Down-regulation of ESRP2 inhibits breast cancer cell proliferation via inhibiting cyclinD1. *Sci. Rep.* **14**, 28475. https://doi.org/10.1038/s41598-024-77980-9 (2024).
50. da Silva, C. M. et al. Studies on free radical scavenging, cancer cell antiproliferation, and calf thymus DNA interaction of schiff bases. *J. Photochem. Photobiol B.* **172**, 129–138. https://doi.org/10.1016/j.jphotobiol.2017.05.020 (2017).
51. Ayaz, M. et al. Biooriented synthesis of Ibuprofen-Clubbed novel Bis-Schiff base derivatives as potential hits for malignant glioma: in vitro anticancer activity and in Silico approach. *ACS Omega*. https://doi.org/10.1021/acsomega.3c07216 (2023). 49228 – 49243.
52. Kaur, H. et al. Diazenyl schiff bases: synthesis, spectral analysis, antimicrobial studies, and cytotoxic activity on human colorectal carcinoma cell line (HCT-116). *Arab. J. Chem.* **13**, 377–392. https://doi.org/10.1016/j.arabjc.2017.05.004 (2020).
53. Cheng, L. X. Antioxidant and antiproliferative activities of hydroxyl-substituted schiff bases. *Bioorg. Med. Chem. Lett.* **20**, 2417–2420. https://doi.org/10.1016/j.bmcl.2010.03.039 (2010).
54. Kanwal, K. et al. Schiff bases of tryptamine as potent inhibitors of nucleoside triphosphate diphosphohydrolases (NTPDases): Structure-activity relationship. *Bioorg. Chem.* **82**, 253–266. https://doi.org/10.1016/j.bioorg.2018.10.046 (2019).
55. Shokrollahi, S., Amiri, A., Fadaei-Tirani, F. & Schenk, K. Promising anti-cancer potency of 4,5,6,7-tetrahydrobenzo[d]thiazole-based Schiff-bases. *J. Mol. Liq.* **300**, 112262. https://doi.org/10.1016/j.molliq.2019.112262 (2020).
56. Chacko, S. & Samanta, S. A novel approach towards design, synthesis, and evaluation of some schiff base analogs of 2-aminopyridine and 2-aminobezothiazole against hepatocellular carcinoma. *Biomed. Pharmacother.* **89**, 162–176. https://doi.org/10.1016/j.biopha.2017.01.108 (2017).
57. Belay, Y. et al. Synthesis, antibacterial activities, cytotoxicity, and molecular Docking studies of salicyledene derivatives. *J. Mol. Struct.* **1275**, 134623. https://doi.org/10.1016/j.molstruc.2022.134623 (2023).
58. Abu-Hashem, A. A., Al-Hussain, S. A. & Design Synthesis of new 1,2,4-Triazole/1,3,4-Thiadiazole with spiroindoline, Imidazo[4,5-b]quinoxaline and Thieno[2,3-d]pyrimidine from Isatin derivatives as anticancer agents. *Mol* **27**, 835. https://doi.org/10.3390/molecules27030835 (2022).
59. Daina, A., Michielin, O. & Zoete, V. SwissADME: a free web tool to evaluate pharmacokinetics, druglikeness and medicinal chemistry friendliness of small molecules. *Sci. Rep.* **7**, 42717. https://doi.org/10.1038/srep42717 (2017).
60. Blois, M. S. Antioxidant determinations by the use of a stable free radical. *Nature* **181**, 1199–1200. https://doi.org/10.1038/1811199a0 (1985).

Acknowledgements

We gratefully acknowledge financial support from the Research Council of the University of Mazandaran.

Author contribution statement

O.R: Methodology; Investigation; Software and Writing–origin draft; Conceptualization and Formal analysis; S.A: Writing–review & editing; Supervision; Project administration; Funding acquisition; Conceptualization; M. T: Writing–review & editing; Project administration; Funding acquisition; A.K: : Formal analysis; S.S: Software; Molecular dynamic simulation.

Declarations

Competing interests

The authors declare that they have no known competing financial interests or personal relationships that could have appeared to influence the work reported in this paper.

Additional information

Supplementary Information The online version contains supplementary material available at https://doi.org/10.1038/s41598-025-91113-w.

Correspondence and requests for materials should be addressed to S.A.

Reprints and permissions information is available at www.nature.com/reprints.

Publisher's note Springer Nature remains neutral with regard to jurisdictional claims in published maps and institutional affiliations.

Open Access This article is licensed under a Creative Commons Attribution-NonCommercial-NoDerivatives 4.0 International License, which permits any non-commercial use, sharing, distribution and reproduction in any medium or format, as long as you give appropriate credit to the original author(s) and the source, provide a link to the Creative Commons licence, and indicate if you modified the licensed material. You do not have permission under this licence to share adapted material derived from this article or parts of it. The images or other third party material in this article are included in the article's Creative Commons licence, unless indicated otherwise in a credit line to the material. If material is not included in the article's Creative Commons licence and your intended use is not permitted by statutory regulation or exceeds the permitted use, you will need to obtain permission directly from the copyright holder. To view a copy of this licence, visit http://creativecommons.org/licenses/by-nc-nd/4.0/.

© The Author(s) 2025